Article

Influence of Boron on the Creep Behavior and the Microstructure of Particle Reinforced Aluminum Matrix Composites

Steve Siebeck [1],*, Kristina Roder [1], Guntram Wagner [1] (ID) **and Daisy Nestler [2]** (ID)

[1] Institute of Materials Science and Engineering, Chemnitz University of Technology, Chair of Composites and Material Compounds, D-09107 Chemnitz, Germany; kristina.roder@mb.tu-chemnitz.de (K.R.); guntram.wagner@mb.tu-chemnitz.de (G.W.)

[2] Fakultät für Maschinenbau, Technische Universität Chemnitz, Professur Strukturleichtbau und Kunststoffverarbeitung, D-09107 Chemnitz, Germany; daisy.nestler@mb.tu-chemnitz.de

* Correspondence: steve.siebeck@mb.tu-chemnitz.de; Tel.: +49-371-531-37531

Abstract: The reinforcement of aluminum alloys with particles leads to the enhancement of their mechanical properties at room temperature. However, the creep behavior at elevated temperatures is often negatively influenced. This raises the question of how it is possible to influence the creep behavior of this type of material. Within this paper, selected creep and tensile tests demonstrate the beneficial effects of boron on the properties of precipitation-hardenable aluminum matrix composites (AMCs). The focus is on the underlying microstructure behind this effect. For this purpose, boron was added to AMCs by means of mechanical alloying. Comparatively higher boron contents than in steel are investigated in order to be able to record their influence on the microstructure including the formation of potential new phases as well as possible. While the newly formed phase Al_3BC can be reliably detected by X-ray diffraction (XRD), it is difficult to obtain information about the phase distribution by means of scanning electron microscopy (SEM) and scanning transmission electron microscopy (STEM) investigations. An important contribution to this is finally provided by the investigation using Raman microscopy. Thus, the homogeneous distribution of finely scaled Al_3BC particles is detectable, which allows conclusions about the microstructure/property relationship.

Keywords: aluminum matrix composites; creep behavior; Raman microscopy; Al_3BC; particle reinforced; powder metallurgy

1. Introduction

Within the Collaborative Research Center 692, a series of particle-reinforced aluminum matrix composites (AMCs) based on a precipitation-hardenable aluminum alloy were produced and investigated. The results on room temperature properties are published in [1–6]. In addition, creep tests were carried out, in which all tested AMCs showed higher creep rates than the unreinforced reference material.

An important mechanism that influences the creep rate of particle-reinforced materials is the acceleration of the precipitation kinetics [7]. Particularly, this is caused by the high dislocation density in the vicinity of the reinforcement particles [8]. The reference material was consolidated analogously to the AMCs by hot isostatic pressing and extrusion. However, it was not high-energy ball milled. This means that in addition to the particle reinforcement itself, the strong strain hardening is a significant difference between the AMCs and the reference material. This is in turn accompanied by the formation of a very fine-grained microstructure. Unlike at the time-independent plastic deformation, a fine-grained structure has a negative effect on the creep behavior. For example, in case of diffusional

creep, the creep rate behaves in inverse proportion to the square of the grain size and in case of grain boundary diffusion even to the cube [9,10]. Furthermore, it was confirmed that the direct effects of the particles compared to the indirect ones by influencing the matrix material is smaller [11].

This correlation was also confirmed by a series of experiments on the creep behavior of the highly plastically deformed reference material by equal channel angular pressing (ECAP) [12]. From this, it can be derived that in addition to grain boundary sliding, diffusion-controlled mechanisms in particular dominate the creep behavior of the investigated AMCs. These include the mechanisms of creep as well as the accelerated precipitation kinetics. Thus, a possible approach to increase the resistance against creep shall be the obstruction of diffusion processes or the stabilization of the grain boundaries. In steels, this is realized by alloying elements with a small atomic radius, such as boron or lithium [13,14].

The resistance against creep is already significantly increased by a boron content in the ppm range [15]. Boron dissolved in austenite has a high binding energy to lattice defects such as dislocations and vacancies and therefore segregates at grain boundaries during cooling [16,17]. This reduces both the grain boundary energy and the diffusivity for iron and carbon along the grain boundaries. Depending on the steel, the precipitation of $M_{23}(B,C)_6$ phases (borocarbides) with epitaxies to the adjacent austenite grains follows. They stabilize the grain boundaries and are able to close cavities [18,19]. The formation of borocarbides may also be considered an indicator of excessive boron contents [20]. No indication can be found in the literature for a specific influence on the creep behavior of aluminum materials by boron. The behavior of the material system aluminum and boron by means of mechanical alloying has already been investigated [21]. When using up to 50 wt % B, the formation of the boride AlB_{10} could be observed.

Within this paper, selected creep and tensile tests demonstrate the beneficial effects of boron on the properties of precipitation-hardenable AMCs. The focus is on the underlying microstructure behind this effect. For this purpose, boron was added to micro-scaled as well as to a nano-scaled SiCp-reinforced AMC. Higher boron contents than in steel are investigated in order to be able to record the influence on the microstructure including the formation of potential new phases. While the newly formed phase Al_3BC can be reliably detected by X-ray diffraction (XRD), it is difficult to obtain optical information about the phase distribution by means of scanning electron microscopy (SEM) and scanning transmission electron microscopy (STEM). An important contribution to this is finally provided by the investigation using Raman microscopy. Thus, the homogeneous distribution of finely scaled Al_3BC particles can be detected, which allows conclusions about the microstructure/property relationship.

2. Materials and Methods

The aluminum alloy that was used as matrix material was supplied in the form of a commercial, gas-atomized, spherical powder with a particle size fraction <100 μm (TLS Technik GmbH & Co. Spezialpulver KG, Bitterfeld, Germany). The chemical composition (in weight-percent) of the alloy was 3.9% Cu, 0.7% Mg, 0.6% Mn, 0.1% Si, 0.2% Fe, balance Al (AA2017). As small particle sizes minimize local stress concentrations in the aluminum matrix, fine-grained SiC alpha phase powder with a fraction of smaller than 1 μm (97.5%, ESK-SIC GmbH, Frechen, Germany) as well as a nano sized beta phase with a fraction smaller than 200 nm (PlasmaChem, Berlin, Germany) were used as reinforcing components.

The composite powder was processed in a water-cooled high-energy ball mill Simoloyer® CM08 (Zoz Company, Wenden, Germany) with ceramic lining. Milling was performed for at least four hours in air atmosphere (closed milling chamber). The remaining oxygen is incorporated into the composite powder and this leads to the formation of finely dispersed spinels ($MgAl_2O_4$) in the bulk material. As the spinels are finely distributed in rather smaller quantities, there is no negative effect expected [22]. Since the powder has non-passivated surfaces after the milling process, there is a possibility of heating. This happens only with an intense supply of oxygen and the reaction is generally moderate due to the

size of the composite particles. However, appropriate precautions should be taken into consideration. Results regarding the influence of the milling atmosphere were published in [2].

The addition of boron was also done by means of high-energy ball milling. Boron particles (>95%, Sigma-Aldrich, St. Louis, MO, USA) with a size of approx. 1 µm have been used for this purpose. The boron particles behave similarly to the ceramic particles within the aluminum matrix. To limit welding of the particles, as well as adhesion to the rotor, balls, and chamber, small amounts of stearic acid (C18H36O2, Merck KGaA, Darmstadt, Germany) were added as process control agent [23]. To remove the stearic acid after milling, the composite powder was first subjected to hot-degassing (450 °C, 6×10^{-2} bar, 4 h). Compaction for all materials was then performed by hot isostatic pressing at 450 °C for 3 h and at a pressure of 1100 bar. Finally, the material was extruded in a temperature range between 355 and 370 °C to produce semi-finished square bars with a cross section of 15×15 mm^2. The extrusion was performed with a punch speed of 2 mm/s and an extrusion ratio of 42:1. Hot isostatic pressing and extrusion were realized by PLM GmbH (Gladbeck, Germany). All materials were solid solution heat treated at 505 °C for at least 60 min, water quenched and naturally aged at room temperature (T4 condition). Details on the preparation of this kind of AMCs are published in [3–5,22,24]. Table 1 shows the composition of the five AMCs that are the subject of this paper.

Table 1. Composition of the investigated AMCs (aluminum matrix composites).

Volume Fraction in vol %		
SiC < 1 µm	SiC < 200 nm	Boron
10	-	-
10	-	0.9
10	-	3.0
-	5	-
-	5	5.0

For the characterization of strength and ductility, cylindrical tensile specimens (with an aspect ratio of the gauge length of three) were machined from the billets in the direction of extrusion. Quasi-static tensile tests were performed at room temperature in a conventional testing machine (Zwick GmbH & Co. KG, Ulm, Germany) with a constant cross-head speed corresponding to an initial strain rate of 10^{-3} s^{-1}. At least three tests were performed for the different material conditions, in particular to provide better statistics on fracture strains of the AMCs.

The creep tests were carried out on a creep testing machine ATS 2330 (ATS Inc., Butler, PA, USA) with a maximum force of 53 kN. All tests were carried out under uniaxial tensile load. The sample geometry was cylindrical with a measuring length of 30 mm and a measuring length diameter of 6 mm. The total length of the samples was 80 mm. They were fastened within the testing machine by means of two ISO metric screw threads (M12). The qualitative creep tests were carried out at a temperature of 180 °C. This corresponds to a homologous temperature of 0.35 of the matrix alloy, which is the maximum service temperature of the AA2017 alloy. The tension used in all experiments was 200 MPa. At least two parallel samples were tested in each case.

Metallographic sections of the bulk material were prepared by mechanical grinding and polishing. The microstructures were analyzed by scanning electron microscopy (SEM) and scanning transmission electron microscopy (STEM) on thin sections using a Neon40 (Zeiss AG, Oberkochen, Germany) field emission microscope operating at 30 kV with energy dispersive X-ray spectroscopy (EDX). The specimens for optical micrograph (OM) analysis were taken from the transverse plane and from the flow plane (i.e., parallel to the direction of extrusion). To determine the phase composition, XRD investigations were performed with a D8 Discover (Bruker Corp., Billerica, MA, USA). The measurements were carried out using a copper K-alpha radiation.

For the additional high-resolution chemical analysis, selected samples were analyzed by flight of time secondary ions mass spectrometry (ToF-SIMS) by tascon GmbH (Münster, Germany).

The minimum diameter of the beam was 300 nm. By recording a spectrum for each sample point, information about the atomic and molecular structure of the outer 1 to 3 monolayers of the solid was obtained. The sensitivities are in the ppm range with a lateral resolution of up to 100 nm.

Raman studies were performed using the inVia Raman microscope (Renishaw, Gloucestershire, UK) with a frequency-doubled Nd:YAG laser having a wavelength of 532 nm, and a maximum power of 100 mW. The advantage of Raman microscopy or Spectroscopy over the X-ray fine structure analysis is that using Raman many spectra within an area of a few 100 µm^2 can be recorded due to scanning with a high spatial resolution. For this purpose, a laser power of 50%, a measuring time per step of 1 s, and a step size of 0.2 µm has been used. The spectra can then be assigned to specific phases based on the characteristic peaks. Finally, using this data, a spatially resolved mapping of the identified phases can be generated. Above all, not only ceramics can be measured using Raman but also intermetallic phases, in contrast to pure metals can be Raman-active. Accordingly, this method provides a useful complement to the microstructural characterization of AMC materials whenever the expected phases and associated Raman spectra are known. The SiC polytype can also be identified by Raman spectroscopy because of its characteristic peaks [25]. This includes the cubic and hexagonal modifications used within this paper.

3. Results and Discussion

3.1. Influene of Boron on the Creep Behavior and Tensile Strength

A boron content of 0.9 vol % slows down the minimum creep rate of the micro-scaled AMCs with 10 vol % volume fraction and prolongs the time to fracture, Figure 1a. Higher boron contents of 3.0 vol % and 5.0 vol % lead to a further marked improvement. It should be noted that the material with a boron content of 5.0 vol % is based on nanoscaled reinforced AMCs (5 vol % SiC particles). However, the reference AMCs without boron achieve similar results in the creep test.

The addition of boron also led to significant improvements in the stress-strain behavior, Figure 1b. Thus, a boron content of 0.9 vol % lead to a similar effect as caused by the increase of the SiC content by about 5 vol % in AMCs. The elongation at break decreased analogously. The further increase to 3.0 vol % boron caused only a relatively small increase in strength but in proportion to lower elongation.
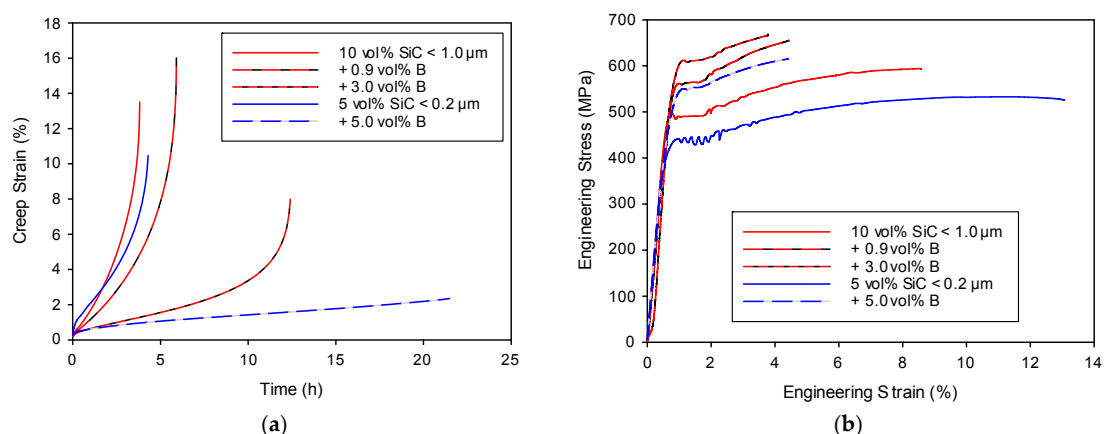

Figure 1. Influence of boron content on selected mechanical properties, based on: (**a**) tensile creep tests at a temperature of 180 °C and a stress of 200 MPa; (**b**) tensile tests.

3.2. Microstructure

In the extruded AMC material (Figure 2) boron-containing phases in the micron range can be detected. Especially on the ion-etched cross sections even smaller ones become visible. In Figure 2b, a boron enrichment at high-angle grain boundaries is possibly recognizable. By means of STEM,

the identification of the boron containing particles succeeds only to a limited extent. There are now even more different phase particles with very small dimensions than in the AMC without boron. Figure 3 confirms the presence of boron by means of STEM on a rather large particle. The figure further illustrates the problem of the phase assignment in the present microstructure.
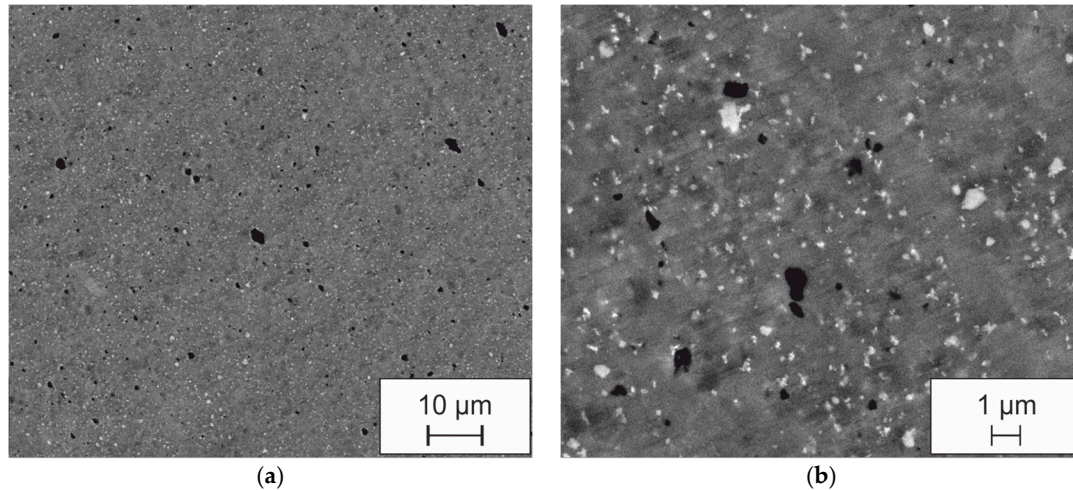

(a) (b)

Figure 2. SEM images (SE) on the ion-etched cross section of an AMC reinforced with 10 vol % SiC and 3 vol % boron; matrix material: AA2017; size of the SiC and B particles: about 1 μm; B-containing phases (black), IM phases (white), SiC particles (hardly contrasted); (**a**,**b**) with different magnification.
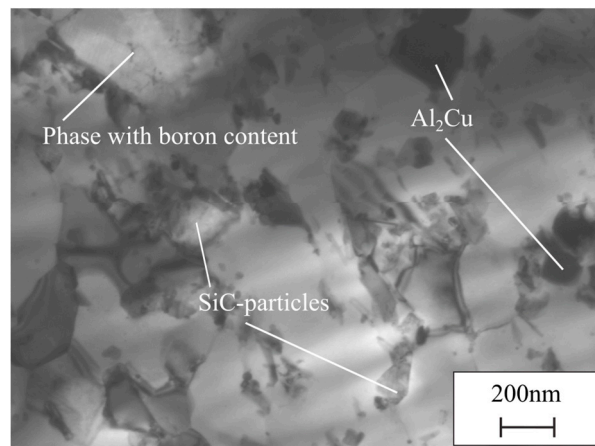

Figure 3. STEM (scanning transmission electron microscopy) image on the cross section of an AMC reinforced with 10 vol % SiC and 3 vol % boron.

In addition to the different structural components, TEM-typical diffraction contrast makes the evaluation of TEM and STEM examinations more difficult. These include different orientation, oblique grain boundaries and interfaces, crystal bendings, and the variation of the preparation thickness. Accordingly, it is probable that in addition to the proven phase, there may possibly be other considerably smaller boron-containing particles. ToF-SIMS investigations seem to be confirming the existence of a fine boron network at the grain boundaries (Figure 4). However, the clear evidence is still missing. The images also suggest that there is an affinity between B and Mg, which leads to the formation of Mg-B particles, presumably MgB_2. By comparison with the results of ToF-SIMS investigations on high energy milled powders, it can be demonstrated that this intermetallic Mg- and B-containing phase is formed at a higher temperature during the powder metallurgy processing and is not yet detectable in the powder stage (Figure 5).
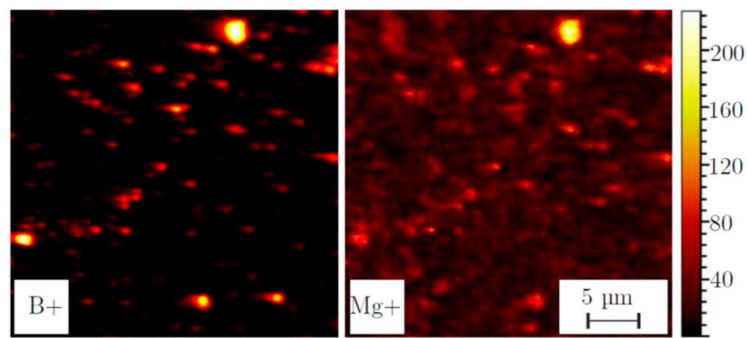
Figure 4. ToF-SIMS (flight of time secondary ions mass spectrometry) mapping on the cross section of an AMC reinforced with 10 vol % SiC and 3 vol % boron; matrix material: AA2017; size of the SiC and B particles: about 1 μm.
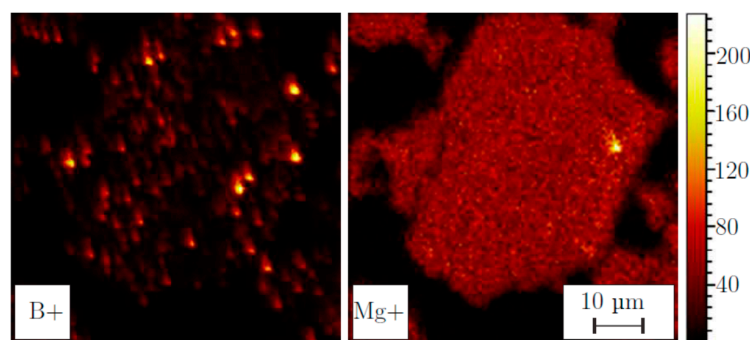

Figure 5. ToF-SIMS mapping on the powder section of composite powder reinforced with 10 vol % SiC and 3 vol % boron; matrix material: AA2017; size of the SiC and B particles: about 1 μm.

A reliable determination of the chemical composition by means of EDX is not possible due to the small size of the phase particles. Due to the low quantity and the low content, detection by XRD examinations is also not successful. However, the aluminum boron carbide phase Al_3BC, which was not yet been found in the powder is detectable (Figure 6).
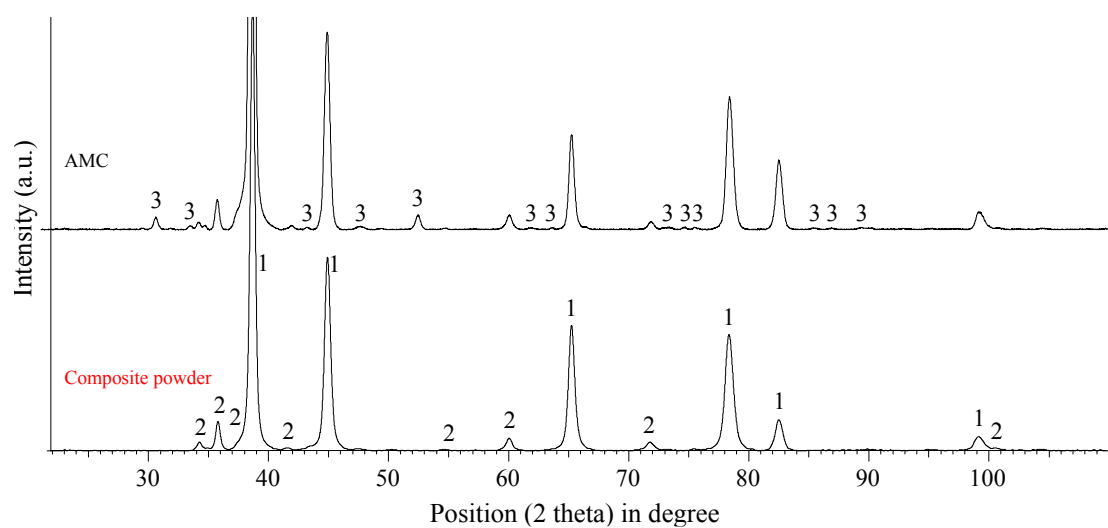

Figure 6. X-ray fine structure analysis of an AMC reinforced with 10 vol % SiC and 3 vol % boron and the underlying composite powder; matrix material: AA2017; size of the SiC and B particles: about 1 μm; 1: Al, 2: SiC, 3: Al_3BC.

The existence of this phase within the samples was confirmed by means of Raman microscopy. The basis for this investigation is the work of Meyer [26,27], who dealt with Raman and infrared spectra of Al_3BC and other ternary aluminum carbides. Figure 7 shows the results of the Raman investigations. The spectra of a sample containing 3 vol % of boron and the corresponding reference AMC without boron are obtained by averaging all the measured spectra within the mapping area. The band used for the evaluation of the false color representation is marked with the corresponding color. The identification of the phase Al_3BC succeeds from the bands detected by Meyer [26,28] at 147, 335, and 520 cm^{-1}.
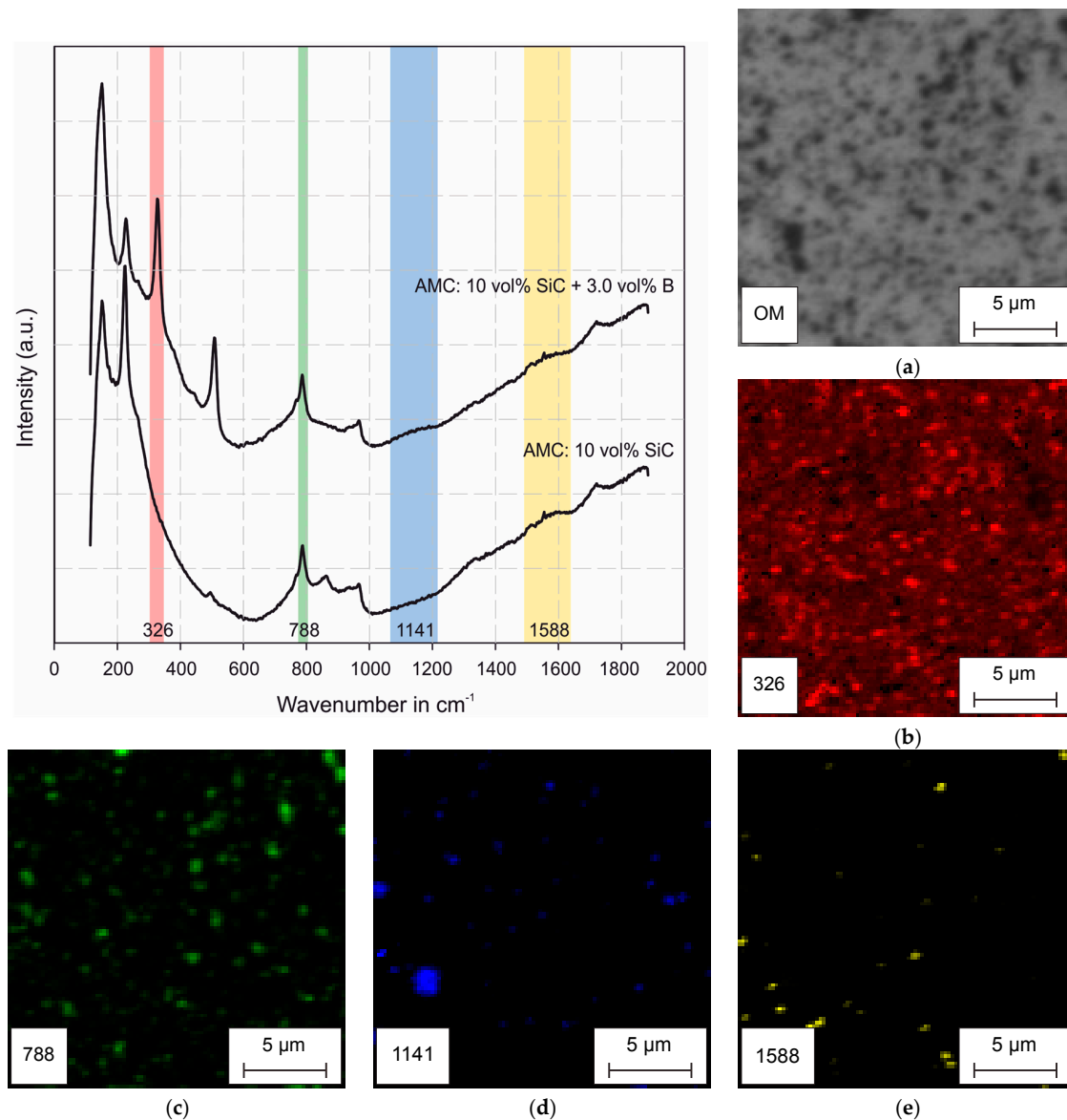

Figure 7. Raman mapping at an AMC with 10 vol % SiC and 3 vol % B and the averaged single spectra of the sample and the reference AMC with 10 vol % SiC; (**a**) optical micrograph of measuring area for mapping by bands: (**b**) at 326 cm^{-1} for Al_3BC, (**c**) at 788 cm^{-1} for SiC, (**d**) at 1141 cm^{-1} for boron, and (**e**) 1588 cm^{-1} for carbon.

The measured bands of the own samples are at 147, 326, and 508 cm^{-1}. This means that with increasing wave numbers they are slightly shifted towards smaller wave numbers. Such peak shifts indicate lattice distortions. In [29], the pressure-dependence of such shifts was investigated and

illustrated by means of the Al_3BC_3 phase. Against this background, the peak shifts appears to be quite plausible with regard to the processing history of the AMCs. Further, in contrast to the finely divided phase particles, which apparently exist in a nanoscale, Meyer [26] recorded the spectra of single crystals with a size of $4 \times 4 \times 0.3$ mm^3. The Al_3BC mapping (red) illustrates the fine distribution by the fact that the selected band is detectable at almost every measuring point of the sample. In addition to Al_3BC, the bands of SiC, boron (B band for comparison in [30]) and carbon were evaluated. The latter is only very isolated and local, but already detectable in unreinforced samples, which was only hot isostatic pressed. Their detectability illustrates the already indicated presence of small amounts of carbon within the milled materials.

Nevertheless, even a small chemical interaction with the SiC particles cannot be ruled out. If the stabilization of the grain boundaries by boron atoms is to be the decisive mechanism of action, the explanation of this behavior would be that the higher boron content leads to a better boron distribution within the material. The fact that steels with significantly lower boron concentrations already produce the desired effect may be due to the atomic distribution at the grain boundaries. For the investigated AMCs, the only possible way to get a good boron distribution at the grain boundaries is through the diffusion processes that occur during powder metallurgical processing and heat treatment. A higher boron content would thus ultimately improve the distribution along the grain boundaries due to shorter diffusion paths and larger concentration differences. On the other hand, the excess of boron content obviously leads to the formation of sufficiently small, well-distributed borocarbide phases. This is the reason why neither the stress-strain behavior nor the creep behavior at elevated temperature is adversely affected. Like any particle reinforcement, they can also have a significant contribution to the creep behavior. This is particularly true if they, unlike precipitations, are thermally stable and thus remain very small.

4. Conclusions

Mechanical alloying has been used to add boron to particle-reinforced aluminum matrix composites. The main goal was to influence the creep behavior towards smaller creep rates. The results of the subsequent investigation of the creep behavior, the tensile strength, and the microstructure lead to the following conclusions:

- The distribution of boron particles succeeds. However, occasionally larger B-particles remain detectable. SEM and ToF-SIMS investigations indicate a fine distribution within the matrix.
- Both the creep resistance as well as the tensile strength increase with increasing boron content within the frame tested.
- By X-ray diffractometry, the newly formed phase Al_3BC can be detected. The existence of the phase can be confirmed by investigations using Raman microscopy. In addition, this makes it possible to visualize the distribution of the phase within the matrix by means of Raman mapping.
- The mechanism behind the improvement in creep resistance is not clear according to the current knowledge. The element boron may affect the diffusivity of the AMCs as well as grain boundary sliding as expected. On the other hand, it is also likely that the phase Al_3BC has a share in the improvement of the tested mechanical properties. After all, it is very small, well distributed, and stable against aging.

Author Contributions: Steve Siebeck is responsible for the production and characterization of the aluminum matrix composites. Kristina Roder accompanied the raman measurements with her professional expertise. Daisy Nestler and Guntram Wagner accompanied the material-technical part of the project and the manuscript with their professional expertise. All authors were involved in the preparation of the final version of the manuscript.

Conflicts of Interest: The authors declare no conflict of interest.

References

1. Hockauf, M.; Wagner, M.F.-X.; Händel, M.; Lampke, T.; Siebeck, S.; Wielage, B. High-strength aluminum-based light-weight materials for safety components-recent progress by microstructural refinement and particle reinforcement. *Int. J. Mater. Res.* **2012**, *103*, 3–11. [CrossRef]
2. Siebeck, S.; Nestler, D.; Podlesak, H.; Wielage, B. Influence of milling atmosphere on the high-energy ball-milling process of producing particle-reinforced aluminum matrix composites. In *Integration of Practice-Oriented Knowledge Technology: Trends and Prospectives*; Fathi, M., Ed.; Springer: Berlin/Heidelberg, Germany, 2013; pp. 315–321.
3. Siebeck, S.; Nestler, D.; Wielage, B. Producing a particle-reinforced AlCuMgMn alloy by means of mechanical alloying. *Materialwiss. Werkstofftech.* **2012**, *43*, 567–571. [CrossRef]
4. Siebeck, S.; Nestler, D.; Wielage, B. Hochenergie-Kugelmahlen zur Herstellung partikelverstärkter AMCs mit hochfester, maßgeschneiderter Aluminummatrix. In *Verbundwerkstoffe, Tagungsband*; Wanner, A., Ed.; Conventus Congressmanagement & Marketing: Jena, Germany, 2013; pp. 115–121.
5. Wagner, S.; Siebeck, S.; Hockauf, M.; Nestler, D.; Podlesak, H.; Wielage, B.; Wagner, M.F.-X. Effect of SiC-reinforcement and equal-channel angular pressing on microstructure and mechanical properties of AA2017. *Adv. Eng. Mater.* **2012**, *14*, 388–393. [CrossRef]
6. Nestler, D.J. *Beitrag zum Thema Verbundwerkstoffe-Werkstoffverbunde. Status quo und Forschungsansätze*; Universitätsverlag Chemnitz: Chemnitz, Germany, 2014.
7. Broeckmann, C.; Packeisen, A. Kriechen einer partikelverstärkten Aluminumlegierung unter Berücksich-tigung des Gefüges. *Metall* **1998**, *52*, 702–711.
8. Dutta, B.; Surappa, M.K. Age-hardening behaviour of Al-Cu-SiCp composites synthesized by casting route. *Scr. Metall. Mater.* **1995**, *32*, 731–736. [CrossRef]
9. Rösler, J.; Harders, H.; Bäker, M. *Mechanisches Verhalten der Werkstoffe, 4*; überarb. und erw. Aufl; Springer: Wiesbaden, Germany, 2012.
10. Bürgel, R. *Handbuch Hochtemperatur-Werkstofftechnik. Grundlagen, Werkstoffbeanspruchungen, Hochtempera-Turlegierungen und-Beschichtungen; mit 70 Tabellen, 3*; überarb. und erw. Aufl; Vieweg: Wiesbaden, Germany, 2006.
11. Rösler, J.; Bao, G.; Evans, A.G. The effects of diffusional relaxation on the creep strength of composites. *Acta Metall. Mater.* **1991**, *39*, 2733–2738. [CrossRef]
12. Härtel, M.; Frint, P.; Abstoss, K.G.; Wagner, M.F.-X. Effect of creep and aging on the precipitation kinetics of an Al-Cu Alloy after one pass of ECAP. *Adv. Eng. Mater.* **2017**, *20*. [CrossRef]
13. Melloy, G.F.; Slimmon, P.R.; Podgursky, P.P. Optimizing the boron effect. *Metall. Trans.* **1973**, *4*, 2279–2289. [CrossRef]
14. Choi, Y.-S.; Kim, S.-J.; Park, I.-M.; Kwon, K.-W.; Yoo, I.-S. Boron distribution in a low-alloy steel. *Met. Mater.* **1997**, *3*, 118–124. [CrossRef]
15. Kim, B.; Yun, H.; Lee, D.; Lim, B. Effect of boron on creep characteristics in 9Cr-1.5Mo alloys. *J. Phys. Conf. Ser.* **2009**, *144*, 12030. [CrossRef]
16. Schriever, U. *Untersuchungen zur Wirkungsweise der Elemente Bor, Titan, Zirkon, Aluminum und Stickstoff in Wasservergüteten, Schweissbaren Baustählen*; Kommission der Europäischen Gemeinschaften, Generaldirek-tion Wissenschaft, Forschung und Entwicklung: Luxemburg, 1991.
17. McMahon, C.J. The role of solute segregation in promoting the hardenability of steel. *Metall. Trans. A* **1980**, *11*, 531–535. [CrossRef]
18. López-Chipres, E.; Mejía, I.; Maldonado, C.; Bedolla-Jacuinde, A.; El-Wahabi, M.; Cabrera, J.M. Hot flow behavior of boron microalloyed steels. *Mater. Sci. Eng. A* **2008**, *480*, 49–55. [CrossRef]
19. Ohmori, Y.; Yamanaka, J. Hardenability of boron-treated low carbon low alloy steels. *Proc. Ann. Symp. Comput. Appl. Med. Care* **1980**, 44–60.
20. Shigesato, G.; Fujishiro, T.; Hara, T. Boron segregation to austenite grain boundary in low alloy steel measured by aberration corrected STEM-EELS. *Mater. Sci. Eng. A* **2012**, *556*, 358–365. [CrossRef]
21. Abenojar, J.; Martinez, M.A.; Velasco, F. Effect of the boron content in the aluminum/boron composite. *J. Alloys Compd.* **2006**, *422*, 67–72. [CrossRef]

22. Nestler, D.; Siebeck, S.; Podlesak, H.; Wagner, S.; Hockauf, M.; Wielage, B. Powder metallurgy of particle-reinforced aluminum matrix composites (AMC) by means of high-energy ball milling. In *Integrated Systems, Design and Technology 2010*; Fathi, M., Holland, A., Ansari, F., Weber, C., Eds.; Springer: Berlin/Heidelberg, Germany, 2011; pp. 93–107.

23. Nestler, D.; Siebeck, S.; Podlesak, H.; Wielage, B.; Wagner, S.; Hockauf, M. Influence of process control agent (PCA) and atmosphere during high-energy ball milling for the production of particle-reinforced aluminum matrix composites. *Materialwiss. Werkstofftech.* **2011**, *42*, 580–584. [CrossRef]

24. Podlesak, H.; Siebeck, S.; Mücklich, S.; Hockauf, M.; Meyer, L.; Wielage, B.; Weber, D. Powder metallurgical fabrication of SiC and Al_2O_3 reinforced Al-Cu alloys. *Materialwiss. Werkstofftech.* **2009**, *40*, 500–505. [CrossRef]

25. Nakashima, S.; Harima, H. Raman investigation of SiC polytypes. *Phys. Stat. Sol.* **1997**, *162*, 39–64. [CrossRef]

26. Meyer, F.D. Festkörperchemische Untersuchungen von Ternären Aluminumcarbiden mit Bor, Silicium und Stickstoff. Doctoral thesis, Albert-Ludwigs-Universität Freiburg, Freiburg, Germany, 1998.

27. Meyer, F.D.; Hillebrecht, H. Synthesis and crystal structure of Al_3BC, the first boridecarbide of aluminum. *J. Alloys Compd.* **1997**, *252*, 98–102. [CrossRef]

28. Madelung, O.; Kück, S.; Werheit, H. *Non-Tetrahedrally Bounded Binary Compounds II, New Series*; Springer: Berlin/Heidelberg, Germany, 2000.

29. Xiang, H.; Li, F.; Li, J.; Wang, J.; Wang, X.; Wang, J.; Zhou, Y. Raman spectrometry study of phase stability and phonon anharmonicity of Al_3BC_3 at elevated temperatures and high pressures. *J. Appl. Phys.* **2011**, *110*, 113504. [CrossRef]

30. Orlovskaya, N.; Lugovy, M. *Boron Rich Solids. Sensors, Ultra High Temperature Ceramics, Thermoelectrics, Armor*; Springer: Dordrecht, The Netherlands, 2011.